NANO LETTERS

pubs.acs.org/NanoLett Letter

Infrared Resonance Raman of Bilayer Graphene: Signatures of Massive Fermions and Band Structure on the 2D Peak

Lorenzo Graziotto,* Francesco Macheda, Tommaso Venanzi, Guglielmo Marchese, Simone Sotgiu, Taoufiq Ouaj, Elena Stellino, Claudia Fasolato, Paolo Postorino, Marvin Metzelaars, Paul Kögerler, Bernd Beschoten, Matteo Calandra, Michele Ortolani, Christoph Stampfer, Francesco Mauri, and Leonetta Baldassarre

Cite This: *Nano Lett.* 2024, 24, 1867−1873 Read Online

ACCESS | Metrics & More | Article Recommendations | Supporting Information

ABSTRACT: Few-layer graphene possesses low-energy carriers that behave as massive Fermions, exhibiting intriguing properties in both transport and light scattering experiments. Lowering the excitation energy of resonance Raman spectroscopy down to 1.17 eV, we target these massive quasiparticles in the split bands close to the **K** point. The low excitation energy weakens some of the Raman processes that are resonant in the visible, and induces a clearer frequency-separation of the substructures of the resonance 2D peak in bi- and trilayer samples. We follow the excitation-energy dependence of the intensity of each substructure, and comparing experimental measurements on bilayer graphene with *ab initio* theoretical calculations, we trace back such modifications on the joint effects of probing the electronic dispersion close to the band splitting and enhancement of electron−phonon matrix elements.

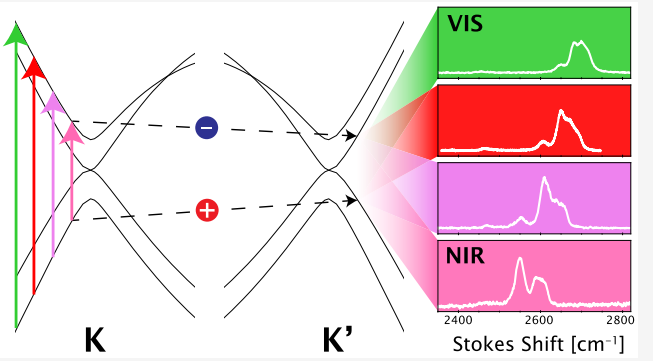

KEYWORDS: *graphene, Raman, electron−phonon, massive Dirac Fermions, transport*

Downloaded via UNIVERSITA DI ROMA LA SAPIENZA on April 11, 2024 at 09:56:07 (UTC).
See https://pubs.acs.org/sharingguidelines for options on how to legitimately share published articles.

Raman scattering can be used as a powerful experimental tool to explore the electron−phonon interaction in two-dimensional (2D) materials.[1] The strength of the electron−phonon coupling (EPC), which is determined by the interplay between atomic displacements and the electronic band structure of the material, can be strongly modified in 2D materials where, due to the reduced dimensions, long-range Coulomb interactions are less efficiently screened.[2−6] By resorting to resonance Raman scattering, i.e., Raman processes involving an electronic transition between two real states of the system under exam, one can obtain high Raman signal also for several modes with nonzero $\mathbf{q}$ wavevectors within the first Brillouin zone (BZ).[7] For example, the Raman spectrum of graphene is composed by a first-order mode at $\mathbf{q} = 0$ (the G peak) and several double-resonance modes (called D, D+D″, 2D, 2D′), which have a wavevector $\mathbf{q} \neq 0$.[8,9] By changing the incoming laser energy ($\epsilon_L = \hbar\omega_L = hc/\lambda_L$), one probes different regions of both the electron and the phonon dispersion, and any variation in the electronic properties (due to number of layers, doping, defects, or strain) is reflected into a modification of the position, the width, and the intensity of the Raman peaks.[10−13]

In references 14 and 15, it was theoretically predicted that in graphene the coupling between carriers in the vicinity of the Dirac point and zone-boundary phonons gets strongly enhanced by Coulomb interactions. Given this theoretical prediction, valid in general for any 2D material displaying Dirac cones, it is of great interest to perform resonance Raman experiments with laser emission in the infrared, in order to excite electron−hole pairs as close as possible to the Dirac point. Indeed, recently,[16] experiments performed on monolayer graphene with laser excitation energies down to $\epsilon_L = 1.17$ eV have shown a large enhancement of the ratio between the 2D and the 2D′ resonance Raman peak intensities, which was explained in terms of a momentum-dependent EPC that is enhanced for carriers interacting with phonons at **K** with respect to those at **Γ**. In a similar fashion, an enhanced EPC could occur also for the massive Fermions of bilayer graphene, where the resonance condition near the bottom of the split bands can be matched[17] with infrared light.

In this work, we show how the line-shape of the 2D peak for bilayer and trilayer graphene is modified with near-infrared (NIR) excitation energy, compared to the line-shape for visible

Received: September 13, 2023
Revised: January 26, 2024
Accepted: January 26, 2024
Published: February 2, 2024

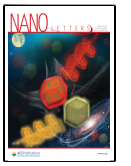

© 2024 American Chemical Society

https://doi.org/10.1021/acs.nanolett.3c03502
Nano Lett. 2024, 24, 1867−1873

(VIS) excitation energy. We find that, for bilayer graphene, such line-shape modification corresponds to a rearrangement of the intensity among the different subpeaks that compose the resonance peak. We compare the resonance Raman spectra on hBN-encapsulated bilayer graphene to *ab initio* calculations and prove that we can spectrally resolve and identify the different resonant scattering pathways within the 2D peak, attempting to understand the origin of the spectral weight shift within the different scattering processes.

We have performed resonance Raman spectra measurements on hBN-encapsulated few-layer graphene for a number of laser excitation energies (wavelengths):

ϵ_L [eV]	1.17	1.58	1.96	2.33	2.54	3.06
λ_L [nm]	1064	785	633	532	488	405

For laser excitation energy $\epsilon_L \geq 1.58$ eV, we have relied on dispersive Raman setups (*Horiba LabRAM HR*, and *WiTec* for 1.58 eV), while $\epsilon_L = 1.17$ eV spectra have been collected with a Michelson interferometer coupled via fibers to an optical microscope (*Bruker MultiRAM*). The spectra have been corrected for the CCD response function or for that of the single-point germanium detector. The spectral calibration for 1.17 eV data is ensured by the interferometric detection scheme, while the other data have been spectrally calibrated with Neon light spectra.

In Figure 1 we report Raman measurements for $\epsilon_L = 1.96$ and 1.17 eV on monolayer, bilayer, and trilayer graphene. As expected, the 2D peak line-shape of bi- and trilayer graphene is built up by several different subpeaks, which we deconvolve with the sum of four (bilayer) or six (trilayer) Baskovian[20] functions $f_B(\omega)$ (see Supporting Information (SI) for definition). We observe in particular that the 2D peak of the bilayer graphene is dramatically modified by lowering the laser excitation energy, as it displays two main features well separated in frequency for $\epsilon_L = 1.17$ eV, which we fit via the sum of three Baskovian functions. The overall 2D peak line-shape of trilayer graphene for $\epsilon_L = 1.17$ eV is also modified with respect to the one for $\epsilon_L = 1.96$ eV, with a larger distance in energy between the center frequencies of its subpeaks, allowing for a better deconvolution of its line-shape, showing four dominant subpeaks instead of six. This spectral evolution is explained in terms of the electronic bands dispersion proper of the different types of few-layer graphene.[21−24] In Bernal-stacked bilayer graphene, the $2p_z$ orbitals of the four carbon atoms in the unit cell hybridize to give rise to two pairs of valence (π_1, π_2) and conduction (π_1^*, π_2^*) bands[25] (depicted in each panel of Figure 2). In Bernal-stacked trilayer graphene, one finds instead three pairs of valence (π_1, π_2, π_3) and conduction bands (π_1^*, π_2^*, π_3^*)[26] (see SI). Although bilayer or trilayer graphene may be viewed just as two or three coupled monolayers and, indeed, in the intrinsic case they possess zero band gap, the low-energy electronic dispersion bears striking differences with respect to the monolayer: the π_1 and π_1^* bands, which are degenerate at the **K** and **K′** points (where in the undoped case the Fermi level lies), display a quadratic behavior with massive quasiparticles, at variance with the massless Fermions in the monolayer's Dirac cones. Moreover, the second pair of bands (π_2, π_2^* in bilayer, π_3, π_3^* in trilayer), which still shows quadratic dispersion, is split at **K** by an energy difference that is estimated to be about $\Delta\epsilon_{split} = 0.7-0.8$ eV in the bilayer[27,28] and 1.2 eV in the trilayer.[19] In Bernal-stacked trilayer graphene, the third pair of bands (π_2, π_2^*) shows the same Dirac cone dispersion of the monolayer.[29] These tangled band structure modifications are mapped into the subpeaks that

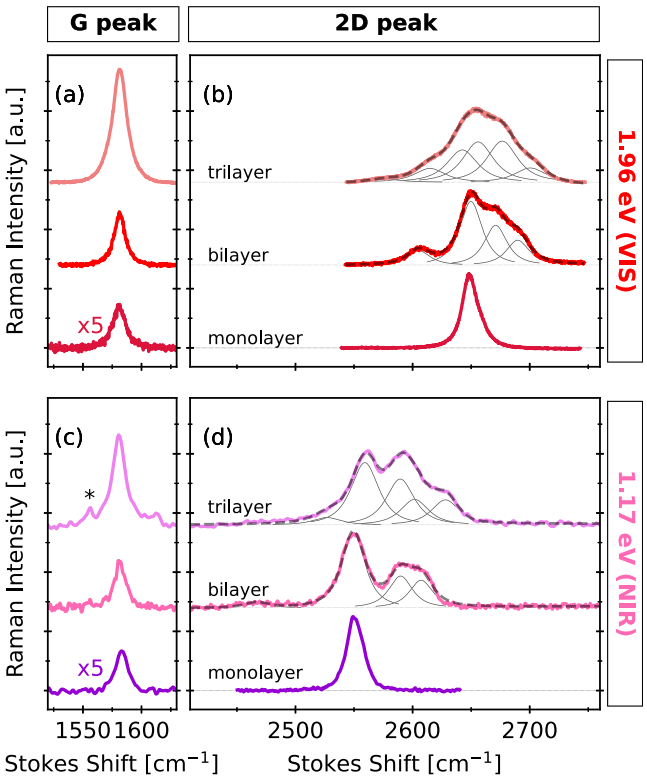

Figure 1. G (a, c) and 2D (b, d) Raman peaks measured with visible (VIS) $\epsilon_L = 1.96$ eV (a, b) and near-infrared (NIR) $\epsilon_L = 1.17$ eV (c, d) for monolayer, bilayer, and trilayer graphene. Each curve has been normalized to the respective height of the 2D peak, and the intensity of the G peak of the monolayer has been multiplied by five for visual clarity. The star near the trilayer's G peak at 1.17 eV indicates a spurious Raman peak due to oxygen molecules. Notice how the shape of the G peak does not vary across the different numbers of layers and excitation energies, while the 2D peak is strongly modified and develops, as the number of layers is increased, features at both higher and lower Stokes shift. These features are fitted via the sum of 4 (bilayer)[18] or 6 (trilayer)[19] Baskovian functions (see Supporting Information). Lowering the excitation energy to $\epsilon_L = 1.17$ eV, these features become better separated in frequency, and some of them are strongly suppressed, in particular in the case of bilayer graphene, where just three Baskovian functions are used.

build up the 2D peak line-shape. The latter arise due to the different resonant scattering pathways between neighboring cones, as pointed out in refs 18 and 26, and are evident in the case of both bilayer and trilayer graphene.

We now focus on the bilayer graphene case, where at $\epsilon_L = 1.17$ eV the separation between subpeaks is more evident, and we show that the three Baskovian subpeaks correspond mainly to two resonant scattering pathways. In order to lighten the notation, in the following we will refer to the four low-energy electronic bands of bilayer graphene by enumerating them in ascending order (with respect to the energy at the **K** point), as labeled on the right side of Figure 2a. As is already understood in refs 18 and 30, the incident laser light of frequency ω_L couples predominantly the two pairs of corresponding bands, i.e., 1 and 4 or 2 and 3, generating electron−hole pairs either in bands 1 and 4 or in bands 2 and 3, with wavevectors close to the **K** point. Subsequently, both the electron and the hole are inelastically scattered by two quasi-degenerate TO phonons[18] (which have opposite wavevectors $\mathbf{q} \sim \mathbf{K}$ to satisfy crystal momentum conservation and have a total energy $\hbar\Omega_{2D} \sim 0.3$ eV for $\epsilon_L = 1.17$

https://doi.org/10.1021/acs.nanolett.3c03502
Nano Lett. 2024, 24, 1867−1873

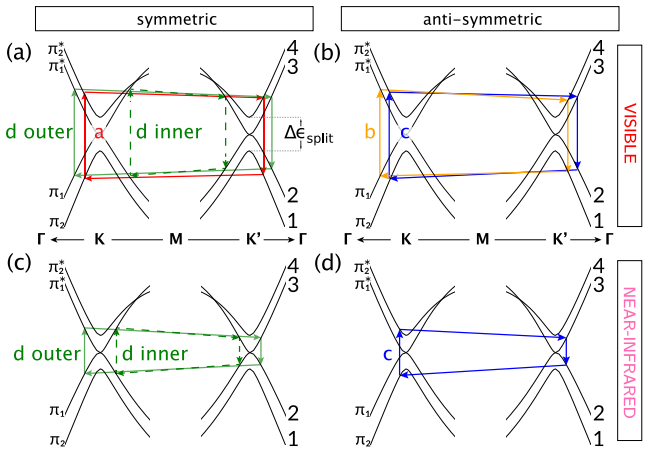

Figure 2. (a–d) Diagrams of the most significant scattering processes that build up the 2D peak in bilayer graphene for visible (a, b) and near-infrared (c, d) excitation energy, involving the electronic bands along the high-symmetry **Γ**–**K**–**M** direction. The labeling 1–4 of the bands follows their energy ordering at the **K** point, while the labeling of the processes separates them in symmetric (processes a and d), where the electron/hole is scattered within the same band, and antisymmetric (processes c and b), where instead the electron/hole changes band upon scattering with the TO phonon. For illustrative purposes, we show only the outer contribution, except for the D process where we further distinguish between inner and outer contributions.

eV, which depends on the excitation energy via the phonon dispersion, see Figure 3c) to the neighborhood of the **K**′ point, either on the same conduction/valence band that they started in (symmetric processes, which are labeled a and d in Figure 2a), or in the other one (antisymmetric processes, labeled c and b in Figure 2b). Finally, the electron and the hole recombine, and a photon with frequency $\omega_L - \Omega_{2D}$ is emitted. The notable aspect of double-resonance Raman processes is that all the intermediate states of the process are real states of the system, hence, the electron–hole pair generation (recombination) must match the energy of the incoming (scattered) photon. This is indeed the case for the four processes that mainly contribute to the 2D peak in the case of visible excitation energies (as depicted in Figure 2a,b). On the other hand, by lowering the excitation energy more to the infrared, the electron–hole pair upon scattering on the TO phonon pair can match the frequency $\omega_L - \Omega_{2D}$ of the scattered photon only if it belongs to the pair of **K**-degenerate bands 2 and 3 or if it has an energy greater than $\Delta\epsilon_{split}$. Thus, while processes c and d are resonantly allowed, a and b are sensitive to the value of $\Delta\epsilon_{split}$ (see SI) and display a strong suppression compared to the case of visible excitation energy (Figure 2c,d). With this understanding, we use 1.17 eV excitation energy with the aim of suppressing the contribution of a and b processes to the 2D peak and then clearly separate in frequency the contributions from c and d (see Figure 1d for bilayer and the discussion below). We point out that while it is customary to resolve the experimental peaks by fitting them with the sum of more than one f_B (as done in Figure 1), these peaks do not immediately refer to the a–d processes described above. Indeed, not only the resonance condition selects phonons with some energy dispersion (determined by the mutual interplay of the electronic and phononic dispersion details[18,31]), but also different processes involving the same phonon can interfere, so that the total intensity will be different from the mere sum of their squared amplitudes. For each of the a–d processes, a simplified treatment[32] addresses the first issue by further distinguishing between inner and outer processes (see Figure 3b). Inner (outer) refers to the process in which the exchanged phonon wavevector **q** lies along the **Γ**–**K**–**M** direction and it is smaller (greater) than **K**. This definition is extended to **q** belonging to the whole BZ in ref 18 (see SI). In the following we only address the experimental subfeatures as the complex sum of the a–d processes, irrespective of the inner and outer distinction, and we compare to the full *ab initio* calculations.[18,31]

It is interesting to investigate experimentally and theoretically the relative intensity of the c and d Raman processes as a function of the laser energy since, for the c process, $\epsilon_L = 1.17$ eV generates electron–hole pairs in the split bands 1 and 4 close to the **K** point and therefore could give us optical access to the EPC near the zone-boundary. In Figure 3a we display the experimental bilayer graphene 2D peak line-shape for several excitation energies between 3.06 and 1.17 eV. Below 2500 cm^{-1} one can also identify the double-resonance D+D″ peak, which involves different phonons with respect to the ones of the 2D peak[33] and blue-shifts with increasing ϵ_L. Lowering the excitation energy, along with the overall red-shift of the 2D peak as a whole, which stems from the TO phonon dispersion, the most notable change is a shift of spectral weight within the peak. At $\epsilon_L = 3.06$ eV the most prominent subpeak is the one at higher Stokes shift, associated with process d, while at 1.17 eV the most relevant contribution comes from the subpeak associated with processes b+c. For $\epsilon_L = 1.96$ and 1.58 eV the subpeak ascribed to the b+c processes becomes progressively more intense with respect to that ascribed to the d process, while the intensity related to the a process appears to remain fairly constant. At $\epsilon_L = 1.17$ eV the b + c subpeak is more intense and well separated from the d subpeak, and it is very hard to identify the presence of a clear feature related to the a process alone, as it overlaps spectrally with the D+D″ peak. Remarkably, we find that for $\epsilon_L = 1.17$ eV the relative intensity of the b+c and d subpeaks is dependent on the application of the back-gate voltage or changing the substrate (see Figure S3 in the SI), suggesting that doping and modifications of $\Delta\epsilon_{split}$ impact the 2D line-shape. One may suppose the intensity of the a and b processes to scale in a similar fashion when $\omega_L - \Omega_{2D}$ becomes close to or smaller than $\Delta\epsilon_{split}$. This in turn would suggest that the shift of the spectral weight between the b+c and the d subpeaks is driven by an enhancement of the c subpeak. One possibility is that the enhancement of the c process could arise because the electron–hole pair is excited close to the band edge due to the increased density of states. A small modification of the band structure could thus impact the intensity of the c process much more than what happens for the d process.

To gain information whether the modification of relative intensity of the subpeaks could be linked also to the strength of the EPC as a function of the exchanged momentum between the electron/hole and the phonon (fixed at each excitation energy by the resonance condition, see Figure 3b) or only to the resonance condition met at the bottom of the split bands, we resort to a comparison with theoretical calculations. It is worth pointing out that the simple double-resonance Raman picture which neglects the dependence of the matrix elements on the electron and phonon momenta[34] is not enough to reproduce the relative intensities of the subpeaks. Indeed we have performed *ab initio* calculations using the fourth-order Fermi golden rule following ref 10. In Figure 4 we compare the experimental 2D peak with the result of *ab initio* calculations, performed following the methodology of refs 18 and 31 and using the *EPIq* software,[35] at $\epsilon_L = 2.33$, 1.96, 1.58, and 1.17 eV. We consider

https://doi.org/10.1021/acs.nanolett.3c03502
Nano Lett. 2024, 24, 1867–1873

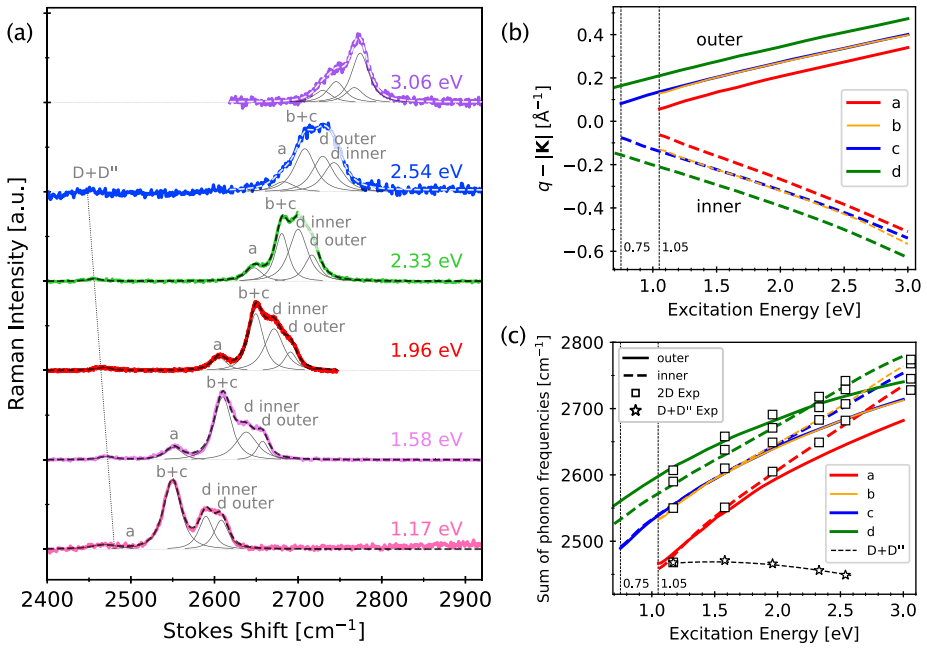

Figure 3. (a) Experimental evolution of the 2D peak line-shape in bilayer graphene for different laser excitation energies. The D+D″ resonance peak is also shown at a lower Stokes shift, and its dispersion can be followed with the guide-to-the-eye dashed line. Notice in particular the dispersion of the 2D peak as a whole (moving in the opposite direction with respect to the D+D″ peak) and the change in spectral weight between its components. Each spectrum has been normalized to its maximum, and the 2D subfeatures have been fitted via the sum of four f_B functions. For $\epsilon_L < 3.0$ eV, the processes referring to the experimental subfeatures are labeled: notice that the b and c processes constructively interfere since they involve the same phonons, and for the d process one can distinguish between the contributions of the inner and outer phonons (which swap places for $\epsilon_L > 2.4$ eV), as discussed in the main text. For higher excitation energies (i.e., 3.06 eV) it becomes harder to attribute a label to each f_B since processes other than the a, b, c, d described in Figure 2 become relevant, and constructively interfere with each other to build up the contribution at higher Stokes shift. Finally, at $\epsilon_L = 1.17$ eV the a subpeak of the 2D peak and the D+D″ peak share similar Stokes shift, and are difficultly separated experimentally. (b) Resonant phonon wavevector $\mathbf{q}$ along $\mathbf{\Gamma}-\mathbf{K}-\mathbf{M}$ as a function of ϵ_L for the different a, b, c, and d processes and inner/outer contributions, as obtained via *ab initio* calculations. Notice that for $\epsilon_L < 1.05$ eV the processes a and b become virtual, since the scattered electron−hole pair cannot recombine resonantly on the split 1−4 bands. Moreover, below the band gap $\Delta\epsilon_{split} = 0.75$ eV also process c is suppressed. Notice also that inner and outer $\mathbf{q}$ process wavevectors become almost symmetric with respect to $\mathbf{K}$ as ϵ_L is reduced since the dispersions approach an isotropic shape. (c) Total frequency Ω_{2D} of the scattered phonon pair with wavevector $\mathbf{q}$ specified in panel **b**, as obtained via *ab initio* calculations for both inner and outer processes (dashed and solid line, respectively) and offset in order to match the experimental data. The square markers represent the central frequencies of the f_B functions with which the experimental data of panel **a** have been fit. The star markers represent instead the frequency of the D+D″ peak. Notice that for $\epsilon_L < 2.0$ eV process d has the inner and outer contributions considerably split in frequency, and that the agreement with the theoretical curves becomes less accurate as ϵ_L is increased, since the simplified inner/outer separation along $\mathbf{\Gamma}-\mathbf{K}-\mathbf{M}$ is not sufficient to describe the shape of the peak.

only these excitation energies since for higher ϵ_L the contribution of processes other than the a, b, c, d discussed above becomes more relevant, giving rise to an increased spectral weight at larger Stokes shift (as evident for the curve measured with ϵ_L = 3.06 eV), which also hinders the interpretation of the experimental subfeatures. The calculations contain DFT only ingredients, apart from the rescaling of the electronic dispersion[10] and the correction to the phonon bands[18] to match GW-corrected results. The inverse lifetime of the intermediate states is evaluated as in ref 18.

For each laser energy, we have calculated the Raman spectra at several different $\Delta\epsilon_{split}$, which are tuned in *ab initio* calculations by the appropriate modification of the carbon interlayer distance (see Figures S5 and S6 in the SI). The total 2D peak and its single contributions a, b, c, and d are shown in Figure 4 for the value $\Delta\epsilon_{split} = 0.75$ eV. From this comparison one can see that these four double-resonance processes are indeed the dominant ones. Moreover, the good agreement in shape between the theoretical curves and the experimental ones for ϵ_L = 2.33, 1.96, and 1.58 eV supports the straightforward identification[18] of the experimental peak subfeatures in terms of the processes depicted in Figure 2a,b. Most notably, for these three spectra, the relative spectral weight of the different subfeatures compares reasonably well between the experimental and theoretical curves. By comparing the evolution of the theoretical spectral weight at several $\Delta\epsilon_{split}$ with that extracted by fitting the experimental data (see Figure S6 in the SI, and Figure 4i for $\Delta\epsilon_{split} = 0.75$ eV), we find that theory overestimates the spectral weight of the b+c process for ϵ_L = 2.33, 1.96, 1.58 eV but always underestimates it at 1.17 eV. At ϵ_L = 1.17 eV (Figure 4d,h) the theoretical line-shape fails in reproducing correctly the spectral weights of the two main features, i.e. the experimental peak is broader and more intense than the theoretical one. The extent of the underestimation of the b+c peak depends on the chosen $\Delta\epsilon_{split}$. However, since the c process involves phonons having wavevectors closer to $\mathbf{K}$ with respect to the d ones (see Figure 3b), one might wonder whether there is an underestimation of peak intensity that arises from a wrong evaluation of the EPC for wavevectors closer to the $\mathbf{K}$ point within the DFT framework, in analogy to what found for monolayer graphene in ref 16. Therein it was argued that such an underestimation could be due to the neglect, proper of DFT, of the dressing of the EPC by Coulomb interaction, but further theoretical investigation is needed to support the hypothesis in the present case, as it would also imply that the massiveness of the Dirac Fermions involved in the

https://doi.org/10.1021/acs.nanolett.3c03502
Nano Lett. 2024, 24, 1867−1873

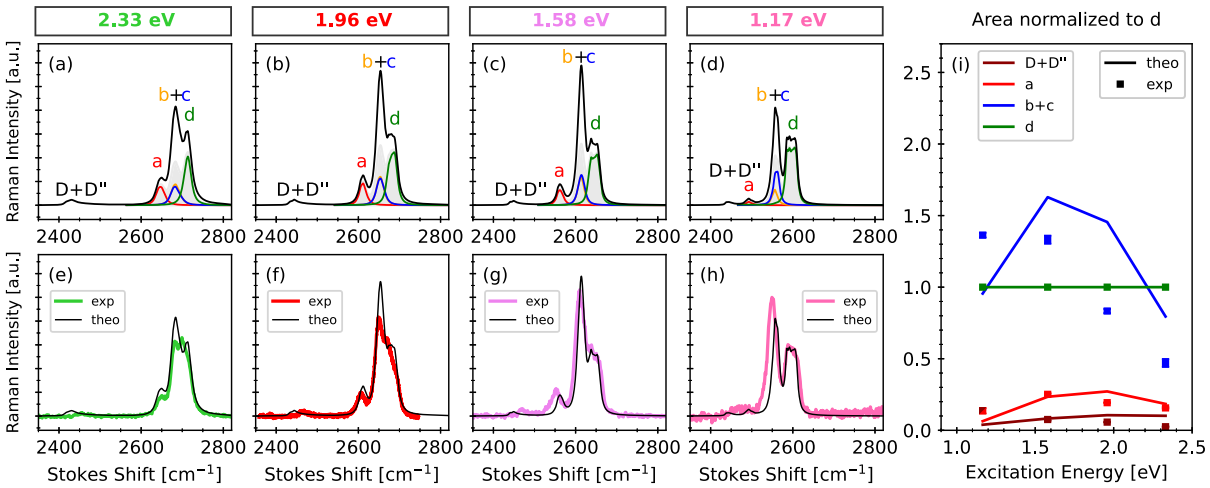

Figure 4. Comparison of the experimental bilayer 2D peak Raman spectra measured at ϵ_L = 2.33, 1.96, 1.58, and 1.17 eV with the results of *ab initio* calculations, where we added an offset to the Stokes shift in order to match the position in frequency. Each spectrum is normalized to the integrated area of its d subpeak. (a−d) Theoretical spectra (black curve), with the peaks related to the processes described in Figure 2a−d (which follow the same labeling and color code): the importance of the quantum interference between the processes is highlighted by the fact that the total intensity (the square of the sum of the amplitudes) is greater than the mere sum of the processes' intensities (gray shaded area). (e−g) Comparison between the theoretical spectrum (solid black) and the experimental 2D peak spectrum (green, red, violet, and pink curves, for ϵ_L = 2.33, 1.96, 1.58, and 1.17 eV, respectively). The theoretical calculations are performed with $\Delta\epsilon_{split}$ = 0.75 eV. Observe how the shape is reproduced fairly good in the case of ϵ_L = 2.33, 1.96 (as first shown in ref 18), and 1.58 eV, while for 1.17 eV, the calculation underestimates the intensity of the b+c processes. (i) Integrated area of the different processes shown in panels a-h normalized to process d, in experiment (squares) and *ab initio* calculations (solid lines). Theoretical results underestimate the b+c process for $\epsilon_L \geq$ 1.58 eV, and they overestimate it for ϵ_L = 1.17 eV.

resonant scattering processes is not a decisive limiting factor for the EPC enhancement.

We can examine other possible causes of the theoretical underestimation of process c with respect to d. Although the magnitude of the contribution of processes a and b is dependent on $\Delta\epsilon_{split}$, we can rule out the possibility that interference with process b can alone explain the enhanced intensity of the b+c subpeak since at this energy also process a, which scales similarly to b, is extremely weak and indistinguishable from the D+D″ peak. Finally, calculations performed by assuming a lower inverse lifetime of the intermediate states give the same results discussed above.

We have shown that by means of resonance Raman spectroscopy with excitation in the infrared, it is possible to suppress the contribution to the Raman spectrum of two of the most relevant scattering pathways building up the double-resonance 2D peak of bilayer graphene in the case of visible excitation. By comparing our experimental results to *ab initio* calculations, we identified the two most important processes contributing to the resonance 2D peak. We found that the relative intensity of the different scattering processes depends on how close to the band edge the electron−hole pair is excited. However, while experimentally the intensity of the b+c peak monotonically increases with respect to the d peak, DFT calculations always predict a decrease in the intensity of the b+c peak at ϵ_L = 1.17 eV. We suggest that such theoretical underestimation of the b+c intensity could stem from an enhancement of the electron−phonon coupling for the processes occurring closer to the **K** point. As a result, we believe that these findings demonstrate how infrared resonance Raman spectroscopy can provide more than a handful of insights into the physics of low-dimensional systems, and we remark that further experimental and theoretical studies are needed to elucidate the dependency of the EPC on the phonon wavevector and the role of Coulomb interactions. This would be of great relevance in order to model the impact of the electron−phonon coupling on the transport and optical properties of low-dimensional systems.[36]

■ ASSOCIATED CONTENT

Supporting Information

The Supporting Information is available free of charge at https://pubs.acs.org/doi/10.1021/acs.nanolett.3c03502.

Contains details on sample processing, laser sources, the definition of the Baskovian fitting function, additional data taken at 1.17 eV excitation energy on hBN-encapsulated bilayer graphene with back-gate voltage applied and on bilayer graphene on the CaF_2 substrate, details on the *ab initio* calculations, the calculated Raman intensity resolved on the phonon wavevectors, calculations performed at different values of the energy split between bands 1−4, and the *ab initio* calculated band structure of the Bernal-stacked trilayer graphene (PDF)

■ AUTHOR INFORMATION

Corresponding Author

Lorenzo Graziotto − *Department of Physics, Sapienza University of Rome, 00185 Rome, Italy;* Present Address: Institute of Quantum Electronics, ETH Zürich, Auguste-Piccard-Hof 1, 8093 Zürich, Switzerland; orcid.org/0000-0002-8049-5079; Email: lgraziotto@phys.ethz.ch

Authors

Francesco Macheda − *Department of Physics, Sapienza University of Rome, 00185 Rome, Italy; Istituto Italiano di Tecnologia, Graphene Labs, 16163 Genoa, Italy*

Tommaso Venanzi − *Department of Physics, Sapienza University of Rome, 00185 Rome, Italy;* orcid.org/0000-0002-6446-7553

https://doi.org/10.1021/acs.nanolett.3c03502
Nano Lett. 2024, 24, 1867−1873

Guglielmo Marchese − *Department of Physics, Sapienza University of Rome, 00185 Rome, Italy;* orcid.org/0000-0002-0732-1320
Simone Sotgiu − *Department of Physics, Sapienza University of Rome, 00185 Rome, Italy;* orcid.org/0000-0001-7889-9763
Taoufiq Ouaj − *JARA-FIT and 2nd Institute of Physics, RWTH Aachen University, 52074 Aachen, Germany*
Elena Stellino − *Department of Physics and Geology, University of Perugia, 06123 Perugia, Italy;* orcid.org/0000-0001-6385-4589
Claudia Fasolato − *Institute for Complex Systems, National Research Council (ISC−CNR), 00185 Rome, Italy;* orcid.org/0000-0003-3450-404X
Paolo Postorino − *Department of Physics, Sapienza University of Rome, 00185 Rome, Italy*
Marvin Metzelaars − *Institute of Inorganic Chemistry, RWTH Aachen University, 52074 Aachen, Germany*
Paul Kögerler − *Institute of Inorganic Chemistry, RWTH Aachen University, 52074 Aachen, Germany;* orcid.org/0000-0001-7831-3953
Bernd Beschoten − *JARA-FIT and 2nd Institute of Physics, RWTH Aachen University, 52074 Aachen, Germany;* orcid.org/0000-0003-2359-2718
Matteo Calandra − *Department of Physics, University of Trento, 38123 Povo, Italy; Istituto Italiano di Tecnologia, Graphene Labs, 16163 Genoa, Italy;* orcid.org/0000-0003-1505-2535
Michele Ortolani − *Department of Physics, Sapienza University of Rome, 00185 Rome, Italy*
Christoph Stampfer − *JARA-FIT and 2nd Institute of Physics, RWTH Aachen University, 52074 Aachen, Germany;* orcid.org/0000-0002-4958-7362
Francesco Mauri − *Department of Physics, Sapienza University of Rome, 00185 Rome, Italy; Istituto Italiano di Tecnologia, Graphene Labs, 16163 Genoa, Italy*
Leonetta Baldassarre − *Department of Physics, Sapienza University of Rome, 00185 Rome, Italy*

Complete contact information is available at: https://pubs.acs.org/10.1021/acs.nanolett.3c03502

Notes

The authors declare no competing financial interest.

■ ACKNOWLEDGMENTS

We acknowledge financial support from the PNRR MUR Project PE0000023-NQSTI. We acknowledge the European Union's Horizon 2020 research and innovation program under Grant Agreement No. 881603-Graphene Core3 and the MORE-TEM ERC-SYN Project, Grant Agreement No. 951215. We acknowledge PRACE for awarding us access to Joliot-Curie Rome at TGCC, France. Part of the calculations were performed on the DECI resource *Mahti CSC* based in Finland at https://research.csc.fi/-/mahti, and part on the ETH *Euler* cluster at https://scicomp.ethz.ch/. L.G. acknowledges funding from the Swiss National Science Foundation (SNF Project No. 200020-207795). T.O., B.B., and C.S. acknowledge funding from the Deutsche Forschungsgemeinschaft (DFG, German Research Foundation) under Germany's Excellence Strategy−Cluster of Excellence Matter and Light for Quantum Computing (ML4Q) EXC 2004/1-390534769. Co-funded by the European Union (ERC, DELIGHT, 101052708). Views and opinions expressed are however those of the authors only and do not necessarily reflect those of the European Union or the European Research Council. Neither the European Union nor the granting authority can be held responsible for them.

■ REFERENCES

(1) Loudon, R. Theory of the resonance Raman effect in crystals. *J. Phys. (Paris)* **1965**, *26*, 677−683.
(2) Sánchez-Portal, D.; Hernández, E. Vibrational properties of single-wall nanotubes and monolayers of hexagonal BN. *Phys. Rev. B* **2002**, *66*, 235415.
(3) Michel, K. H.; Verberck, B. Theory of elastic and piezoelectric effects in two-dimensional hexagonal boron nitride. *Phys. Rev. B* **2009**, *80*, 224301.
(4) Attaccalite, C.; Wirtz, L.; Lazzeri, M.; Mauri, F.; Rubio, A. Doped graphene as tunable electron- phonon coupling material. *Nano Lett.* **2010**, *10*, 1172−1176.
(5) Sohier, T.; Gibertini, M.; Calandra, M.; Mauri, F.; Marzari, N. Breakdown of Optical Phonons' Splitting in Two-Dimensional Materials. *Nano Lett.* **2017**, *17*, 3758−3763.
(6) Macheda, F.; Sohier, T.; Barone, P.; Mauri, F. Electron-phonon interaction and phonon frequencies in two-dimensional doped semiconductors. *Phys. Rev. B* **2023**, *107*, 094308.
(7) Cardona, M. *Light Scattering in Solids I: Introductory Concepts*; Topics in Applied Physics; Springer: Berlin; Heidelberg, 1982.
(8) Ferrari, A. C.; Meyer, J. C.; Scardaci, V.; Casiraghi, C.; Lazzeri, M.; Mauri, F.; Piscanec, S.; Jiang, D.; Novoselov, K. S.; Roth, S.; et al. Raman spectrum of graphene and graphene layers. *Phys. Rev. Lett.* **2006**, *97*, 187401.
(9) Malard, L.; Pimenta, M. A.; Dresselhaus, G.; Dresselhaus, M. Raman spectroscopy in graphene. *Phys. Rep.* **2009**, *473*, 51−87.
(10) Venezuela, P.; Lazzeri, M.; Mauri, F. Theory of double-resonant Raman spectra in graphene: Intensity and line shape of defect-induced and two-phonon bands. *Phys. Rev. B* **2011**, *84*, 035433.
(11) Graf, D.; Molitor, F.; Ensslin, K.; Stampfer, C.; Jungen, A.; Hierold, C.; Wirtz, L. Spatially resolved Raman spectroscopy of single- and few-layer graphene. *Nano Lett.* **2007**, *7*, 238−242.
(12) Martins Ferreira, E. H.; Moutinho, M. V. O.; Stavale, F.; Lucchese, M. M.; Capaz, R. B.; Achete, C. A.; Jorio, A. Evolution of the Raman spectra from single-, few-, and many-layer graphene with increasing disorder. *Phys. Rev. B* **2010**, *82*, 125429.
(13) Neumann, C.; Reichardt, S.; Venezuela, P.; Drögeler, M.; Banszerus, L.; Schmitz, M.; Watanabe, K.; Taniguchi, T.; Mauri, F.; Beschoten, B.; et al. Raman spectroscopy as probe of nanometre-scale strain variations in graphene. *Nat. Commun.* **2015**, *6*, 8429.
(14) Basko, D.; Aleiner, I. Interplay of Coulomb and electron-phonon interactions in graphene. *Phys. Rev. B* **2008**, *77*, 041409.
(15) Lazzeri, M.; Attaccalite, C.; Wirtz, L.; Mauri, F. Impact of the electron-electron correlation on phonon dispersion: Failure of LDA and GGA DFT functionals in graphene and graphite. *Phys. Rev. B* **2008**, *78*, 081406.
(16) Venanzi, T.; Graziotto, L.; Macheda, F.; Sotgiu, S.; Ouaj, T.; Stellino, E.; Fasolato, C.; Postorino, P.; Mišeikis, V.; Metzelaars, M.; et al. Probing enhanced electron-phonon coupling in graphene by infrared resonance Raman spectroscopy. *Phys. Rev. Lett.* **2023**, *130*, 256901.
(17) Malard, L. M.; Nilsson, J.; Elias, D. C.; Brant, J. C.; Plentz, F.; Alves, E. S.; Castro Neto, A. H.; Pimenta, M. A. Probing the electronic structure of bilayer graphene by Raman scattering. *Phys. Rev. B* **2007**, *76*, 201401.
(18) Herziger, F.; Calandra, M.; Gava, P.; May, P.; Lazzeri, M.; Mauri, F.; Maultzsch, J. Two-Dimensional Analysis of the Double-Resonant 2D Raman Mode in Bilayer Graphene. *Phys. Rev. Lett.* **2014**, *113*, 187401.
(19) Cong, C.; Yu, T.; Sato, K.; Shang, J.; Saito, R.; Dresselhaus, G. F.; Dresselhaus, M. S. Raman characterization of ABA-and ABC-stacked trilayer graphene. *ACS Nano* **2011**, *5*, 8760−8768.

(20) Basko, D. M. Theory of resonant multiphonon Raman scattering in graphene. *Phys. Rev. B* **2008**, *78*, 125418.
(21) Grüneis, A.; Attaccalite, C.; Wirtz, L.; Shiozawa, H.; Saito, R.; Pichler, T.; Rubio, A. Tight-binding description of the quasiparticle dispersion of graphite and few-layer graphene. *Phys. Rev. B* **2008**, *78*, 205425.
(22) Mak, K. F.; Sfeir, M. Y.; Misewich, J. A.; Heinz, T. F. The evolution of electronic structure in few-layer graphene revealed by optical spectroscopy. *Proc. Natl. Acad. Sci. U. S. A.* **2010**, *107*, 14999−15004.
(23) Coletti, C.; Forti, S.; Principi, A.; Emtsev, K. V.; Zakharov, A. A.; Daniels, K. M.; Daas, B. K.; Chandrashekhar, M.; Ouisse, T.; Chaussende, D.; et al. Revealing the electronic band structure of trilayer graphene on SiC: An angle-resolved photoemission study. *Phys. Rev. B* **2013**, *88*, 155439.
(24) Popov, V. N. Two-phonon Raman bands of bilayer graphene: Revisited. *Carbon* **2015**, *91*, 436−444.
(25) McCann, E.; Koshino, M. The electronic properties of bilayer graphene. *Rep. Prog. Phys.* **2013**, *76*, 056503.
(26) Torche, A.; Mauri, F.; Charlier, J.-C.; Calandra, M. First-principles determination of the Raman fingerprint of rhombohedral graphite. *Physical Review Materials* **2017**, *1*, 041001.
(27) Kuzmenko, A.; Van Heumen, E.; Van Der Marel, D.; Lerch, P.; Blake, P.; Novoselov, K.; Geim, A. Infrared spectroscopy of electronic bands in bilayer graphene. *Phys. Rev. B* **2009**, *79*, 115441.
(28) Zhang, L. M.; Li, Z. Q.; Basov, D. N.; Fogler, M. M.; Hao, Z.; Martin, M. C. Determination of the electronic structure of bilayer graphene from infrared spectroscopy. *Phys. Rev. B* **2008**, *78*, 235408.
(29) Bao, W.; Jing, L.; Velasco, J., Jr; Lee, Y.; Liu, G.; Tran, D.; Standley, B.; Aykol, M.; Cronin, S.; Smirnov, D.; et al. Stacking-dependent band gap and quantum transport in trilayer graphene. *Nat. Phys.* **2011**, *7*, 948−952.
(30) Ferrari, A. C.; Basko, D. M. Raman spectroscopy as a versatile tool for studying the properties of graphene. *Nat. Nanotechnol.* **2013**, *8*, 235−246.
(31) Graziotto, L.; Macheda, F.; Sohier, T.; Calandra, M.; Mauri, F. Theory of infrared double-resonance Raman spectrum in graphene: the role of the zone-boundary electron-phonon enhancement. *arXiv:2310.09188v2 [cond-mat.mes-hall]* **2023**, na.
(32) Berciaud, S.; Li, X.; Htoon, H.; Brus, L. E.; Doorn, S. K.; Heinz, T. F. Intrinsic line shape of the Raman 2D-mode in freestanding graphene monolayers. *Nano Lett.* **2013**, *13*, 3517−3523.
(33) May, P.; Lazzeri, M.; Venezuela, P.; Herziger, F.; Callsen, G.; Reparaz, J. S.; Hoffmann, A.; Mauri, F.; Maultzsch, J. Signature of the two-dimensional phonon dispersion in graphene probed by double-resonant Raman scattering. *Phys. Rev. B* **2013**, *87*, 075402.
(34) Thomsen, C.; Reich, S. Double Resonant Raman Scattering in Graphite. *Phys. Rev. Lett.* **2000**, *85*, 5214−5217.
(35) Marini, G.; Marchese, G.; Profeta, G.; Sjakste, J.; Macheda, F.; Vast, N.; Mauri, F.; Calandra, M. epiq: An open-source software for the calculation of electron-phonon interaction related properties. *Comput. Phys. Commun.* **2024**, *295*, 108950.
(36) Novoselov, K.; Mishchenko, A.; Carvalho, A.; Castro Neto, A. 2D materials and van der Waals heterostructures. *Science* **2016**, *353*, aac9439.

https://doi.org/10.1021/acs.nanolett.3c03502
Nano Lett. 2024, 24, 1867−1873